Spin-polarized two-dimensional t_{2g} electron gas: Ab initio study of EuO interface with oxygen-deficient SrTiO_{3}

Lingyuan Gao and Alexander A. Demkov

Phys. Rev. B **97**, 125305 — Published 19 March 2018

DOI: 10.1103/PhysRevB.97.125305

Spin-polarized two-dimensional t_{2g} electron gas: *ab-initio* study of EuO interface with oxygen-deficient $SrTiO_3$

Lingyuan Gao and Alexander A. Demkov[1]

Department of Physics, The University of Texas at Austin, Austin, TX, 78712, USA

Abstract

Using first-principles calculations we predict the existence of a spin-polarized two-dimensional electron gas at the interface of a ferromagnetic insulator EuO and oxygen-deficient $SrTiO_3$. The carriers are generated by oxygen vacancies in $SrTiO_3$near the interface and have predominantly Ti-t_{2g} orbital character. At the interface, the split-off d_{xy}-derived conduction band of $SrTiO_3$ is fully spin-polarized and the in-gap vacancy-induced state, found below the conduction band edge, is aligned ferromagnetically with EuO. The calculations suggest a possible mechanism for generating spin-polarized 2DEG for spintronic applications.

Introduction

With a rapidly growing interest in transition metal oxides, perovskite $SrTiO_3$ (STO) stands out as a substrate of choice in oxide epitaxy, and for the important role it plays among the oxide heterojunctions and interfaces. The best known example is arguably the $LaAlO_3/SrTiO_3$ interface. Though comprised of two wide-band-gap insulators it shows a two-dimensional electron gas (2DEG) [1,2] that exhibits a host of intriguing phenomena, including magnetism [3] and superconductivity [4], as well as their coexistence [5,6]. After a decade-long research effort, the mechanism behind the 2DEG formation at this interface is still under debate. The "intrinsic" one (the so-called "polar catastrophe" [7]) refers to electron transfer from the polar oxide ($LaAlO_3$) surface to the interface. While the "extrinsic" mechanism points to oxygen vacancies [8,9] that are one of the most common doping defects during the film growth in ultra-high vacuum and to interface cation exchange [10–12]. The purely vacancy-related 2DEG has been observed at the interface of STO and γ-Al_2O_3 [13,14]. And 2DEG is also observed at the bare STO (001) surface, where it is attributed to oxygen vacancies [15,16]. Interestingly, in this case, along with the 2DEG, an in-gap state is observed 1.3 eV below the Fermi level by an angle-integrated photoemission measurement [16]. On the other hand, an in-gap level 2.7 eV above the valence band edge is observed for the SrO-terminated surface with scanning tunneling spectroscopy [17].

[1] E-mail: demkov@physics.utexas.edu

The controversial role of oxygen vacancies in STO has drawn much attention and has been investigated using density functional theory (DFT) [18–23]. Recently, the Anderson impurity model [24] and DFT plus dynamical-mean field theory (DMFT) [25] applied to an O_v reached qualitative agreement with each other and experiment, suggesting that itinerant t_{2g}–derived states do coexist with a localized in-gap e_g–derived state in bulk oxygen-deficient $SrTiO_3$.

EuO is a ferromagnetic semiconductor with the Curie temperature T_c of 69 K [26]. The large magnetic moment of 7 μ_B on Eu ions originates from the half-filled *4f* states and causes a large spin-split of the conduction *5d* band of 0.6 eV [27]. Spin-polarized 2DEG in the Eu *5d* band has been predicted at the $LaAlO_3$/EuO interface [28,29]. Due to this spin polarization, EuO has potential applications in spin-filter tunneling junctions [30,31]. Theoretically, EuO has been proposed to induce ferromagnetic ordering in graphene and transition-metal dichalcogenide monolayers by the proximity effect that could open a 36 meV exchange-splitting gap in graphene, and lift the valley degeneracy and create a giant valley splitting (over 300 meV) in $MoTe_2$ [32,33]. Recent reports discuss successful growth of graphene on EuO [34,35], making this an intriguing possibility.

Posadas et al., have discussed the ability of many metals to scavenge oxygen from STO at high temperatures [36]. Eu has been demonstrated to form epitaxial EuO layers on STO when deposited in UHV at 300ºC, leaving an oxygen deficient layer of STO below the interface. This opens an intriguing possibility. In this paper, using first-principles theory at the DFT+U level, we propose an alternative approach to creating spin-polarized 2DEG at the interface of oxygen-deficient STO and EuO. The carriers are generated by the oxygen vacancies on the STO side, similar to what is found at the γ-Al_2O_3/STO interface [13,14] rather than by the polar field in the case of $LaAlO_3$ [23]. Also, unlike the previous work, here the carriers would reside not in the Eu *5d* states but mostly in Ti-derived t_{2g} states of STO, and polarization is induced via a proximity effect due to EuO. An e_g in-gap O_v-induced state found below the conduction band edge is singly occupied and aligned ferromagnetically with Eu.

Method

We perform DFT calculations within the generalized gradient approximation (GGA) [37] and projected augmented wave pseudopotentials [38], using Vienna Ab-Initio Simulation

Package [39]. For Sr, Ti, Eu and O, $4s^2 4p^6 5s^2$, $3s^2 3p^6 4s^2 3d^2$, $5s^2 5p^6 4f^7 6s^2$ and $2s^2 2p^4$ are included, respectively. To properly describe the Eu *4f* orbitals, the GGA+U approach [40,41] is employed with an empirical value of $U_f = 5.0$ eV. We use a 17-electron configuration for Eu (*4f* orbitals are not frozen in the core). The calculated EuO lattice constant of 5.164 Å agrees well with the experimental value of 5.144 Å. To include electron correlation in $SrTiO_{3-\delta}$, a combination of $U_d = 5.0$ eV and $J_d = 0.64$ eV is used for the Ti *3d* orbitals [42]. The calculated bulk lattice constant of STO is 3.958 Å. This overestimates slightly the experiment value of 3.905 Å as typical for GGA. The calculated 2.4 eV band gap is still smaller than the experimental value of 3.2 eV; nevertheless, these parameters provide a reasonable description of an oxygen vacancy in STO [18,20,43–45]. As will be discussed later, the U value for Eu does not affect the present results significantly, while that for Ti indeed requires a careful consideration. To model the epitaxial $SrTiO_{3-\delta}$/EuO (001) structure, we employ periodically repeated symmetric slabs $(EuO)_3/TiO_2$-$(SrO\text{-}TiO_2)_6/(EuO)_3$ separated by a thick vacuum region (in access of 20Å). As for the in-plane geometry, the rock salt EuO cell is rotated by 45° to match the perovskite that is understood as being a substrate. This results in an 8.5% tensile strain in EuO. In previous reports, it has been suggested that a tensile strain may induce an in-plane ferroelectricity in EuO [46,47]. The reader interested in the effects of strain in oxide epitaxy is referred to an excellent review by Schlom et al. [48]. However, as it is beyond the intended scope of this work, we preserve the in-plane symmetry and only allow oxygen relaxation along the z direction, normal to the interface. To consider the role of oxygen vacancies in STO, we employ a 2×2 STO supercell (Figure 1 (b)), where a single vacancy is created. We use 600 eV as the plane-wave cutoff energy and sample the Brillouin zone with $4 \times 4 \times 1$ Monkhorst-Pack *k*-point grids [49]. The entire structure is relaxed until the residual force is smaller than 0.02 eV/Å.

As shown in Figure 1 (a), there are two obvious possible epitaxial interfaces between EuO and $SrTiO_3$: (1) Eu is above a hollow site in the TiO_2 plane as a continuation of the Sr sub-lattice (top-H) and (2) Eu is above oxygen in the TiO_2 plane to maintain the Eu-O chain (top-O). As the number of atoms needed to model these interfaces is the same for both types, we can simply compare their total energies in order to decide, which one is more stable. We find the top-H interface to be more stable by 4886 mJ/m^2, and in the rest of the paper we focus on this structure. An oxygen vacancy can be created in the sub-interface SrO plane as shown in Figure 1 (b). The

vacancy formation energy is estimated to be 5.63 eV, close to 5.66 eV calculated for a stand-alone $2 \times 2 \times 4$ $SrTiO_3$ supercell. If a vacancy is created in the interfacial TiO_2 plane, the formation energy is 6.37 eV. This suggests that EuO layers have a small influence on the formation of an oxygen vacancy in $SrTiO_3$. However, the presence of metallic Eu layer would lower the formation energy of a vacancy [50,51].

Results and discussion

We start our discussion with the $(EuO)_3/TiO_2$-$(SrO\text{-}TiO_2)_6/(EuO)_3$ heterostructure (top-H) without a vacancy. Figures 2 (a) and (b) show the density of states (DOS) projected on specific atoms for each layer of this heterostructure. Owing to a mirror-symmetry of the cell, the results for one half of the simulation cell are presented. The system is insulating as expected, since no carriers are introduced. In the EuO layers, the majority-spin Eu *4f* states seen right below the Fermi level (there is a weak hybridization with the oxygen *p* states). This band becomes evanescent in the STO region across the interface. It decays into the STO band gap and disappears at the second TiO_2 layer, 6 Å away from the interface. Also, a EuO surface state right above the top of the oxygen-derived valence band is clearly seen for both spin channels. This state decays slowly and is even recognized at the interfacial layer due to a modest thickness of the EuO region in our simulation. The minority spin empty Eu *4f* states are much higher in energy, beyond the energy window in Figure 2. On the other hand, the EuO conduction band edge is composed mainly of the spin-up Eu *5d* states, and demonstrates the spin-splitting of about 0.6 eV, similar to that in bulk ferromagnetic EuO [28]. In STO, the valence band top is oxygen-dominated and is 1.7 eV below the Fermi level (this suggests a 1.7 eV valence band offset between the two oxides). The STO conduction band bottom is 0.6 eV above the *Fermi level*. The corresponding theoretical band gaps of STO and EuO are 2.3 eV and 0.6 eV, respectively.

We now introduce an oxygen vacancy in the sub-interface SrO plane, as shown in Figures 2 (c) and (d), and the system becomes metallic. In EuO, the valence band top is shifted down to -0.7 eV relative to the *Fermi level* and the conduction band bottom is also 0.1 eV below the *Fermi level*. In STO, the valence band top is shifted down in energy to -2.5 eV. At the interface, the Ti-derived conduction band bottom is at -0.3 eV while in the other three Ti layers, the conduction band edge is at -0.2 eV (all energies are with respect to the *Fermi level*). We also find that a

localized in-gap state is created at the vacancy position in the sub-interface SrO layer. It resides on Ti atoms adjacent to the vacancy site (the interface TiO_2 layer and TiO_2 layer right below the vacancy). One electron is trapped in this in-gap state. As has been discussed by Lin and Demkov, in bulk STO, the vacancy-induced localized state can trap at most one electron, while the second electron occupies the conduction band due to electron-electron repulsion [24]. Also, Hou et al. discussed a similar scenario [20]. The result has also been reproduced by Jeschke et al. using DFT+U [45], however their calculation was restricted to a nonmagnetic case and required multiple vacancies to be arranged in a specific way. Interestingly, in our case, the in-gap state appears only in the spin-up channel, and is aligned ferromagnetically with the Eu ions above the interface. This in-gap state decays quickly into both the STO and EuO regions on both sides of the interface. In EuO, the evanescent states can be seen two layers away from interface. The decay length is estimated as 7.8 Å and 9.3 Å for $SrTiO_3$ and EuO, respectively.

The orbital decomposition of the Ti *d* states for each STO layer is shown in Figure 3 (a). The in-gap vacancy state has mainly a $d_{3z^2-r^2}$ orbital character, mixed with the Ti 4p_z and *s* orbitals due to lifting of the local cubic symmetry caused by the vacancy [52]. This increases the spatial extent of Ti orbitals sufficiently far to introduce coupling between the Ti ions adjacent to the vacancy in layers 3 and 4 (interface). At the interface, the d_{xy} state is shifted down in energy from the other t_{2g} states (d_{xz}/d_{yz}) and is the only one occupied, while in the bulk-like STO region (layer 1), the d_{xz}/d_{yz} states tend to be occupied similarly to d_{xy}. This is similar to the $LaAlO_3/SrTiO_3$ system and has been attributed to the symmetry lowering and orbital reconstruction at the interface [53–56]. In addition, for all 4 Ti ions at the interface, the d_{xy} state has a spin-splitting of about 0.3 eV and only the spin-up channel (same spin as Eu and a vacancy level) is occupied resulting in a spin polarized interface channel.

We compute the total number of itinerant carriers (excluding the e_g vacancy state) $n = n^{\uparrow} + n^{\downarrow}$ and spin polarization $p = \frac{n^{\uparrow} - n^{\downarrow}}{n^{\uparrow} + n^{\downarrow}}$ for each layer. Thus computed number of carriers *n* (per 2x2 STO area) and corresponding spin polarization *p* from layer 1 to layer 4 are 0.22 e^-, 0.2 e^-, 0.13 e^-, 0.19 e^-, and 0%, 8.7%, 30.7% and 100%, respectively. To calculate the number of carriers in each layer, we integrate each atomic orbital-projected DOS from the conduction band edge to the Fermi level, and then sum over all orbitals and atoms in that layer. As there are spaces between atoms (spheres used for the projection), after the projection a small fraction of electron is lost.

On the other hand, if we do the integral using the total DOS (no layer projection), the number is indeed 1. The number of carriers in different layers doesn't change much, while the spin polarization increases significantly when approaching the interface. Note, that the Ti d_{xy} state could carry more electrons compared with the spin-split Eu *5d* band, the DOS of which is rather low. Therefore, the current regime may have an advantage for generating spin-polarized 2DEG over previously suggested schemes, where doping occurs in the EuO layers [28, 29]. To better understand the origin of the spin-split of the interfacial d_{xy} state, we perform the following computational experiment. We consider the same $(EuO)_3/TiO_2$-$(SrO\text{-}TiO_2)_6/(EuO)_3$ heterostructure (top-H) but without vacancies and artificially introduce two extra electrons (a homogeneous compensating background charge is added to maintain the neutrality). The resulting partial DOS projected on the Ti ions is shown in Figure 3 (b). There are no vacancy-related in-gap states, but we still see spin polarization in the d_{xy} band at the interface. This suggests that interfacial states are influenced by the 7 μ_B magnetization of the neighbouring Eu ions and the spin-polarization of 2DEG is caused by the proximity effect (superexchange).

The effect of U: As we use the on-site Coulomb repulsion U on both Eu *4f* states and Ti *3d* states, the theory is not completely ab-initio. And it is important to understand the influence of these semi-empirical parameters on the results of the calculations. Within the DFT+U formalism, the orbital energy ε_i' could be written as $\varepsilon_i' = \varepsilon_i + U(\frac{1}{2} - n_i)$, where ε_i is the orbital energy of the regular LDA/GGA functional, *U* is the Coulomb repulsion and n_i is the orbital occupation [41]. Since the spin-up Eu *4f* states form the valence band, increasing the Eu *U* value would shift the occupied spin-up *4f* states down and the *f-d* band gap would increase accordingly. This agrees well with the calculation; for a Eu U value of 5.0 eV, the band gap is 0.6 eV, and the valence band offset between the Eu *4f* states and O *p* states of STO is 1.7 eV. While with a Eu *U* value of 8.0 eV, the band gap of EuO is 1.2 eV and the valence band offset decreases to 1.1 eV. Apart from that, the band structure doesn't change significantly, including the EuO conduction band edge comprised of Eu *5d* states.

However, when we vary the Ti *U* value, the effect is quite different: Figure 4 shows the DOS projected onto each atomic layer in top-H heterostructure with vacancy while using Ti U = 8 eV. The in-gap state now is completely filled by two electrons from the vacancy and there are no itinerant electrons. Also, instead of being ferromagnetic as in the case of U = 5 eV, the spins on

two Ti ions adjacent to the vacancy prefer the antiferromagnetic arrangement. For Ti ion close to the interface, the spin is aligned ferromagnetically with the Eu ion.

To explain this result, we use a three-orbital model following Lin et al.'s [24]:

$$H = \varepsilon_1 \sum_{\sigma=\uparrow,\downarrow} (n_{1\sigma} + n_{2\sigma}) - g\mu_B H \sum_{i=1,2} (n_{i\uparrow} - n_{i\downarrow}) - t \sum_{\sigma=\uparrow,\downarrow} c_{1\sigma}^{+} c_{2\sigma} - t \sum_{\sigma=\uparrow,\downarrow} c_{1\sigma} c_{2\sigma}^{+}$$
$$+ U \sum_{i=1,2} n_{i\uparrow} n_{i\downarrow} + \varepsilon_0 \sum_{\sigma=\uparrow,\downarrow} n_{0\sigma} - g\mu_B H (n_{0\uparrow} - n_{0\downarrow}).$$

Here, 0 represents the uncorrelated bath orbital with energy ε_0 (for convenience we set ε_0 to 0). Indices 1 and 2 refer to two Ti $d_{3z^2-r^2}$-based localized orbitals with energy ε_1, which are adjacent to vacancy. The hopping parameter t describes the coupling between them and the on-site repulsion U is applied to both orbitals. Furthermore, g is the g factor, μ_B is the Bohr magneton and H is the "external" magnetic field coming from Eu ions. As one vacancy provides two electrons, we need to determine two-electron ground state of this Hamiltonian. There are three possibilities for the ground state: (I) both electrons occupy the itinerant orbital; (II) one electron occupies localized orbital, and the other occupies itinerant orbital; (III) two electrons occupy two localized orbitals. For phase (I), the lowest energy E_I is 0. For phase (II), the lowest energy E_{II} is $\varepsilon_1 - 2g\mu_B H - t$. In the lowest energy configuration, spins of both electrons are aligned along the magnetic field. For phase (III), there are two different lowest energies:

$$E_{III} = 2\varepsilon_1 - g\mu_B H, \;\; E'_{III} = 2\varepsilon_1 + \frac{1}{2}\left(U - \sqrt{U^2 + 16t^2}\right),$$

E_{III} corresponds to a configuration where each electron occupies one localized orbital and spins are ferromagnetically aligned, parallel to the magnetic field. $E_{III}{}'$ corresponds to a configuration where the spins of two electrons are antiferromagnetically aligned, which is the singlet for a two-site Hubbard model [57]. In terms of our DFT calculation, "0" represents the itinerant d_{xy} band while "1" and "2" refer to the localized impurity state. Since ε_1 is larger than ε_0 (which is equal to 0), $E_{II} < E_{III}$. Also, as approximated in [24], $\varepsilon_1 - t$ is smaller than 0, hence $E_{II} < 0 = E_I$. Thus we shall only focus on configurations related to E_{II} and $E_{III}{}'$. Phenomenologically, the DFT result with Ti U =5.0 eV corresponds to E_{II} configuration while U = 8.0 eV corresponds to $E_{III}{}'$ configuration. This shows that for U = 5 eV, E_{II} is lower than $E_{III}{}'$. In the large U limit, $E_{III}{}'$ can

be approximated as $2\varepsilon_1 - \frac{4t^2}{U}$ and if we increase U, E_{III}' would increase while E_{II} remains the same, provided that other parameters are fixed. This suggests that for a larger U, the ground state should remain in phase II, which is contrary to what we find from the DFT calculation. An alternative possibility is that ε_1 shifts down with the increasing U. This could make E_{III}' lower than E_{II} and then the ground state configuration corresponds to E_{III}'. To clarify this, we plot the DOS for the Ti-derived t_{2g} and e_g bands in bulk $SrTiO_3$ for U = 5.0 eV and U = 8.0 eV in Figure 5. For U =8.0 eV, the t_{2g}-e_g splitting indeed becomes smaller by 0.2 eV compared to that obtained using U = 5.0 eV. This will cause ε_1 to be even lower and Ti $d_{3z^2-r^2}$-based localized orbital to shift further down in energy relative to d_{xy} orbital. We note this shift only occurs in DFT and we conclude the ground state should be phase (II). According to Lin et al. [50], the two-peak structure of the Ti $3d_{3z^2-r^2}$ density of states (DOS) corresponds to the bonding and antibonding combinations of Ti-Ti $3d_{3z^2-r^2}$-based orbitals and the separation between the peaks is twice the hopping parameter $2t$. When we compare the partial density of states projected on the Ti ion adjacent to a vacancy in a $2 \times 2 \times 4$ $SrTiO_3$ supercell for U = 5 eV and U = 8 eV, the separation is approximately 2.2 eV in both cases. This suggests that t has a fairly weak dependence on U.

We estimate the magnitude of the EuO-generated magnetic field H by comparing the electronic structure of the oxygen-deficient $SrTiO_3$ with and without EuO layers. For a magnetic system under external magnetic field, the majority band will have a $g\mu_B H$ energy down-shift relative to the minority band. For Ti ion adjacent to vacancy in a $2 \times 2 \times 4$ $SrTiO_3$ supercell, $d_{xy\downarrow}$ is aligned with $d_{xy\uparrow}$. While in Figure 3(a), in the presence of EuO, the interfacial $d_{xy\uparrow}$ band is shifted down 0.3 eV relatively to the $d_{xy\downarrow}$ band, suggesting a $g\mu_B H$ value of 0.3 eV.

Conclusions

In summary, using first-principles calculations we predict a spin-polarized 2DEG at the TiO_2/EuO interface of EuO and an oxygen-deficient $SrTiO_3$. Carriers are residing mostly at the $SrTiO_3$ side of the interface and the strong spin polarization is induced by a proximity effect from the ferromagnetic insulator EuO**.** In addition, a vacancy-induced localized state appears within the band gap of STO just below the conduction band edge. This system provides a robust mechanism for generating spin-polarized 2DEG, which can possibly be used in spintronic

applications, and it may have an advantage as unlike the conduction band of EuO that of STO can host a large number of carriers owing to a higher density of states.

Acknowledgements

We thank K. J. Kormondy and C. Lin for helpful discussions and A. B. Posadas for critically reading the manuscript. Support for this work was provided through the Scientific Discovery through Advanced Computing (SciDAC) program funded by U.S. Department of Energy, Office of Science, Advanced Scientific Computing Research and Basic Energy Sciences under award number DESC0008877 and by the Air Force Office of Scientific Research (FA9550-12-10494).

References

[1] A. Ohtomo and H. Y. Hwang, Nature **427**, 423 (2004).

[2] S. Thiel, G. Hammerl, A. Schmehl, C. W. Schneider and J. Mannhart, Science **313**, 1942 (2006).

[3] A. Brinkman, M. Huijben, M. van Zalk, J. Huijben, U. Zeitler, J. C. Maan, W. G. van der Wiel, G. Rijnders, D. H. a Blank, and H. Hilgenkamp, Nat. Mater. **6**, 493 (2007).

[4] N. Reyren, S. Thiel, A. D. Caviglia, L. F. Kourkoutis, G. Hammerl, C. Richter, C. W. Schneider, T. Kopp, A.-S. Rüetschi, D. Jaccard, M. Gabay, D. A. Muller, J.-M. Triscone, and J. Mannhart, Science **317**, 1196 (2007).

[5] L. Li, C. Richter, J. Mannhart, and R. C. Ashoori, Nat. Phys. **7**, 762 (2011).

[6] J. A. Bert, B. Kalisky, C. Bell, M. Kim, Y. Hikita, H. Y. Hwang, and K. a. Moler, Nat. Phys. **7**, 767 (2011).

[7] N. Nakagawa, H. Y. Hwang, and D. A. Muller, Nat. Mater. **5**, 204 (2006).

[8] A. Kalabukhov, R. Gunnarsson, J. Börjesson, E. Olsson, T. Claeson, and D. Winkler, Phys. Rev. B **75**, 121404 (2007).

[9] G. Herranz, M. Basletić, M. Bibes, C. Carrétéro, E. Tafra, E. Jacquet, K. Bouzehouane, C. Deranlot, A. Hamzić, J.-M. Broto, A. Barthélémy, and A. Fert, Phys. Rev. Lett. **98**,

216803 (2007).

[10] L. Qiao, T. C. Droubay, V. Shutthanandan, Z. Zhu, P. V Sushko, and S. A. Chambers, J. Phys. Condens. Matter **22**, 312201 (2010).

[11] S. A. Chambers, M. H. Engelhard, V. Shutthanandan, Z. Zhu, T. C. Droubay, L. Qiao, P. V. Sushko, T. Feng, H. D. Lee, T. Gustafsson, E. Garfunkel, A. B. Shah, J. M. Zuo, and Q. M. Ramasse, Surf. Sci. Rep. **65**, 317 (2010).

[12] L. Qiao, T. C. Droubay, T. C. Kaspar, P. V. Sushko, and S. A. Chambers, Surf. Sci. **605**, 1381 (2011).

[13] K. J. Kormondy, A. B. Posadas, T. Q. Ngo, S. Lu, N. Goble, J. Jordan-Sweet, X. P. A. Gao, D. J. Smith, M. R. McCartney, J. G. Ekerdt, and A. A. Demkov, J. Appl. Phys. **117**, 95303 (2015).

[14] T. Q. Ngo, N. J. Goble, A. Posadas, K. J. Kormondy, S. Lu, M. D. McDaniel, J. Jordan-Sweet, D. J. Smith, X. P. A. Gao, A. A. Demkov, and J. G. Ekerdt, J. Appl. Phys. **118**, 115303 (2015).

[15] A. F. Santander-Syro, O. Copie, T. Kondo, F. Fortuna, S. Pailhès, R. Weht, X. G. Qiu, F. Bertran, A. Nicolaou, A. Taleb-Ibrahimi, P. Le Fèvre, G. Herranz, M. Bibes, N. Reyren, Y. Apertet, P. Lecoeur, A. Barthélémy, and M. J. Rozenberg, Nature **469**, 189 (2011).

[16] W. Meevasana, P. D. C. King, R. H. He, S.-K. Mo, M. Hashimoto, A. Tamai, P. Songsiriritthigul, F. Baumberger, and Z.-X. Shen, Nat. Mater. **10**, 114 (2011).

[17] W. Sitaputra, N. Sivadas, M. Skowronski, D. Xiao, and R. M. Feenstra, Phys. Rev. B **91**, 205408 (2015).

[18] D. D. Cuong, B. Lee, K. M. Choi, H. Ahn, S. Han, and J. Lee, Phys. Rev. Lett. **98**, 115503 (2007).

[19] Y. S. Kim, J. Kim, S. J. Moon, W. S. Choi, Y. J. Chang, J.-G. Yoon, J. Yu, J.-S. Chung, and T. W. Noh, Appl. Phys. Lett. **94**, 202906 (2009).

[20] Z. Hou and K. Terakura, J. Phys. Soc. Japan **79**, 114704 (2010).

[21] C. Mitra, C. Lin, J. Robertson, and A. A. Demkov, Phys. Rev. B **86**, 155105 (2012).

[22] J. Shen, H. Lee, R. Valentí, and H. O. Jeschke, Phys. Rev. B **86**, 195119 (2012).

[23] A. Lopez-Bezanilla, P. Ganesh, and P. B. Littlewood, Phys. Rev. B **92**, 115112 (2015).

[24] C. Lin and A. A. Demkov, Phys. Rev. Lett. **111**, 217601 (2013).

[25] F. Lechermann, W. Heckel, O. Kristanovski, and S. Müller, Phys. Rev. B **95**, 195159 (2017).

[26] A. Mauger and C. Godart, Phys. Rep. **141**, 51 (1986).

[27] J. Schoenes and P. Wachter, Phys. Rev. B **9**, 3097 (1974).

[28] J. Lee, N. Sai, and A. A. Demkov, Phys. Rev. B **82**, 235305 (2010).

[29] Y. Wang, M. K. Niranjan, J. D. Burton, J. M. An, K. D. Belashchenko, and E. Y. Tsymbal, Phys. Rev. B **79**, 212408 (2009).

[30] P. G. Steeneken, L. H. Tjeng, I. Elfimov, G. A. Sawatzky, G. Ghiringhelli, N. B. Brookes, and D.-J. Huang, Phys. Rev. Lett. **88**, 47201 (2002).

[31] T. S. Santos and J. S. Moodera, Phys. Rev. B **69**, 241203 (2004).

[32] H. X. Yang, A. Hallal, D. Terrade, X. Waintal, S. Roche, and M. Chshiev, Phys. Rev. Lett. **110**, 46603 (2013).

[33] J. Qi, X. Li, Q. Niu, and J. Feng, Phys. Rev. B **92**, 121403 (2015).

[34] A. G. Swartz, P. M. Odenthal, Y. Hao, R. S. Ruoff, and R. K. Kawakami, ACS Nano **6**, 10063 (2012).

[35] J. C. Leutenantsmeyer, A. A. Kaverzin, M. Wojtaszek, and B. J. van Wees, 2D Mater. **4**, 14001 (2016).

[36] A. B. Posadas, K. J. Kormondy, W. Guo, P. Ponath, J. Geler-Kremer, T. Hadamek, and A. A. Demkov, J. Appl. Phys. **121**, 105302 (2017).

[37] J. P. Perdew, K. Burke, and M. Ernzerhof, Phys. Rev. Lett. **77**, 3865 (1996).

[38] P. E. Blöchl, Phys. Rev. B **50**, 17953 (1994).

[39] G. Kresse and J. Furthmüller, Phys. Rev. B **54**, 11169 (1996).

[40] V. I. Anisimov, J. Zaanen, and O. K. Andersen, Phys. Rev. B **44**, 943 (1991).

[41] V. I. Anisimov, F. Aryasetiawan, and A. I. Lichtenstein, J. Phys. Condens. Matter **9**, 767 (1997).

[42] E. Pavarini, S. Biermann, A. Poteryaev, A. I. Lichtenstein, A. Georges, and O. K. Andersen, Phys. Rev. Lett. **92**, 176403 (2004).

[43] M. Choi, F. Oba, and I. Tanaka, Phys. Rev. Lett. **103**, 185502 (2009).

[44] Y. S. Kim, J. Kim, S. J. Moon, W. S. Choi, Y. J. Chang, J.-G. Yoon, J. Yu, J.-S. Chung, and T. W. Noh, Appl. Phys. Lett. **94**, 202906 (2009).

[45] H. O. Jeschke, J. Shen, and R. Valentí, New J. Phys. **17**, 23034 (2015).

[46] E. Bousquet, N. A. Spaldin, and P. Ghosez, Phys. Rev. Lett. **104**, 37601 (2010).

[47] W.-Y. Tong, H.-C. Ding, Y.-C. Gao, S.-J. Gong, X. Wan, and C.-G. Duan, Phys. Rev. B **89**, 64404 (2014).

[48] D. G. Schlom, L.-Q. Chen, C.-B. Eom, K. M. Rabe, S. K. Streiffer, and J.-M. Triscone, Annu. Rev. Mater. Res. **37**, 589 (2007).

[49] H. J. Monkhorst and J. D. Pack, Phys. Rev. B **13**, 5188 (1976).

[50] A. A. Demkov, Phys. Rev. B **74**, 85310 (2006).

[51] A. B. Posadas, K. J. Kormondy, W. Guo, P. Ponath, J. Geler-Kremer, T. Hadamek, and A. A. Demkov, J. Appl. Phys. (2017).

[52] C. Lin, C. Mitra, and A. A. Demkov, Phys. Rev. B **86**, 161102 (2012).

[53] R. Pentcheva and W. E. Pickett, Phys. Rev. B **74**, 35112 (2006).

[54] R. Pentcheva and W. E. Pickett, Phys. Rev. Lett. **99**, 16802 (2007).

[55] J. Lee and A. A. Demkov, Phys. Rev. B **78**, 193104 (2008).

[56] J.-S. Lee, Y. W. Xie, H. K. Sato, C. Bell, Y. Hikita, H. Y. Hwang, and C.-C. Kao, Nat. Mater. **12**, 703 (2013).

[57] J. Hubbard, Proc. R. Soc. A Math. Phys. Eng. Sci. **276**, 238 (1963).

FIGURE CAPTIONS

Figure 1. (color online) The simulation cell of $(EuO)_3/TiO_2$-$(SrO$-$TiO_2)_6/(EuO)_3$ heterostructure. (a) Top view of two different types of interfaces: Eu on top of a hollow site in a TiO_2 plane (top-H) and on top of an oxygen in a TiO_2 plane (top-O); (b) 2×2 supercell with a single vacancy at the sub-interface SrO plane. Only half of the cell is presented due to mirror symmetry. The oxygen vacancy site is marked in black.

Figure 2. (color online) Density of states (DOS) projected on a specific atom for each layer in top-H heterostructure without and with a vacancy. Only the results for the upper half cell are shown due to symmetry. Eu, O, Ti, Sr states are marked by magenta, red, dark blue and green, respectively. EuO surface states are indicated with the square. (a) and (c) panels correspond to the spin-up while (b) and (d) correspond to spin-down components, respectively.

Figure 3 (color online) DOS projected on the Ti *d* states in each layer. Layer 1 represents the central "bulk" part of $SrTiO_3$, while layer 4 represents the interfacial layer. (a) DOS of top-H heterostructure with a vacancy; (b) DOS of top-H heterostructure without vacancies but artificially doped with two extra electrons.

Figure 4 (color online) Similar to Figure 2, the atom-projected DOS for each layer in he heterostructure containing a vacancy with $U_{Ti\text{-}d} = 8$ eV**.**

Figure 5 (a) The e_g-t_{2g} splitting in bulk $SrTiO_3$ for $U_{Ti\text{-}d} = 5$ eV and (b) $U_{Ti\text{-}d} = 8$ eV**.**

Figures

Figure 1

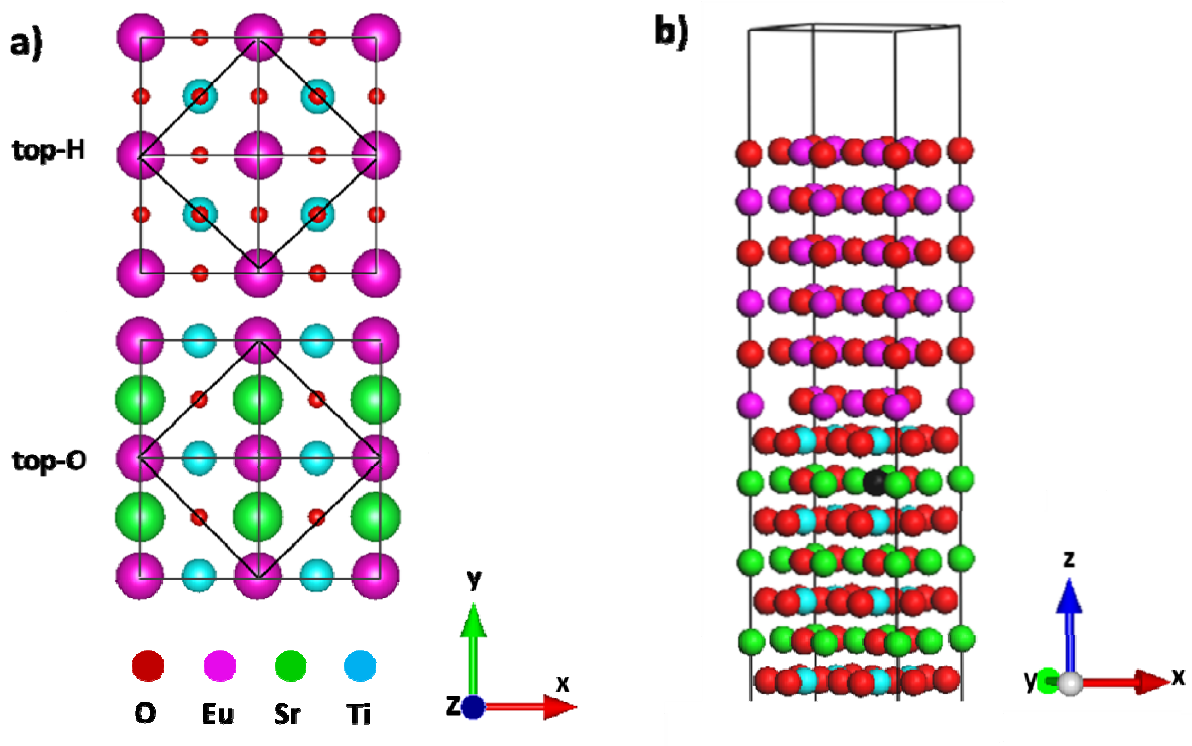

Figure 2

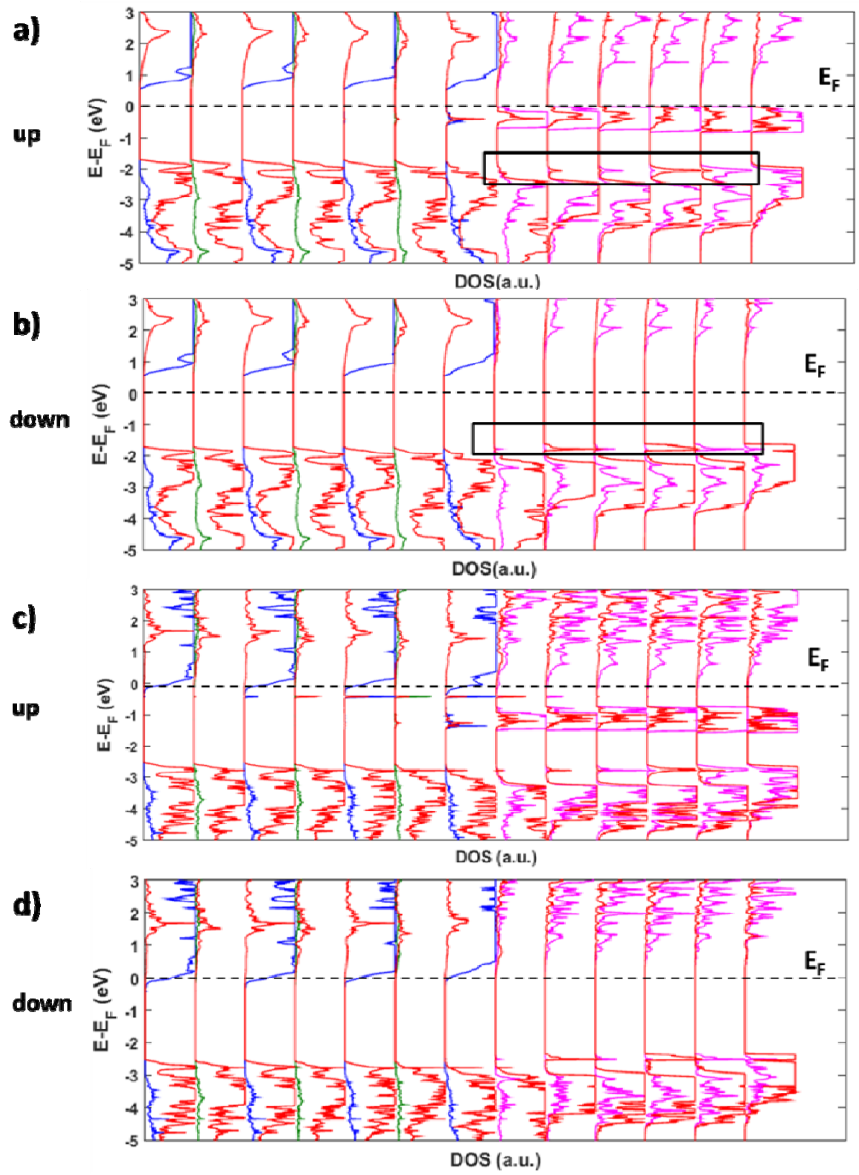
a)
up
E-E_F (eV)
E_F
DOS(a.u.)
b)
down
E-E_F (eV)
E_F
DOS(a.u.)
c)
up
E-E_F (eV)
E_F
DOS (a.u.)
d)
down
E-E_F (eV)
E_F
DOS (a.u.)

Figure 3

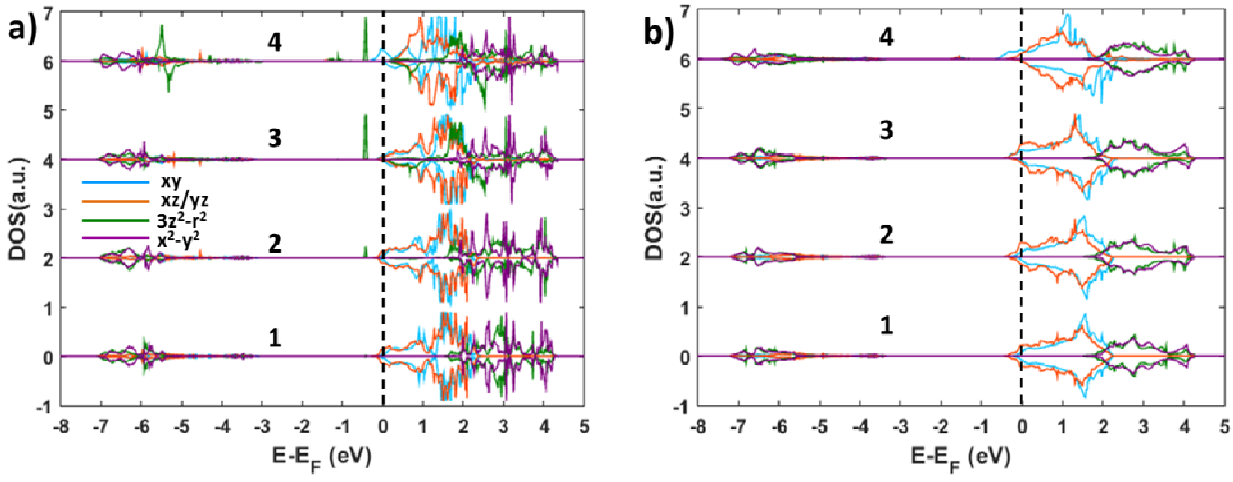

Figure 4

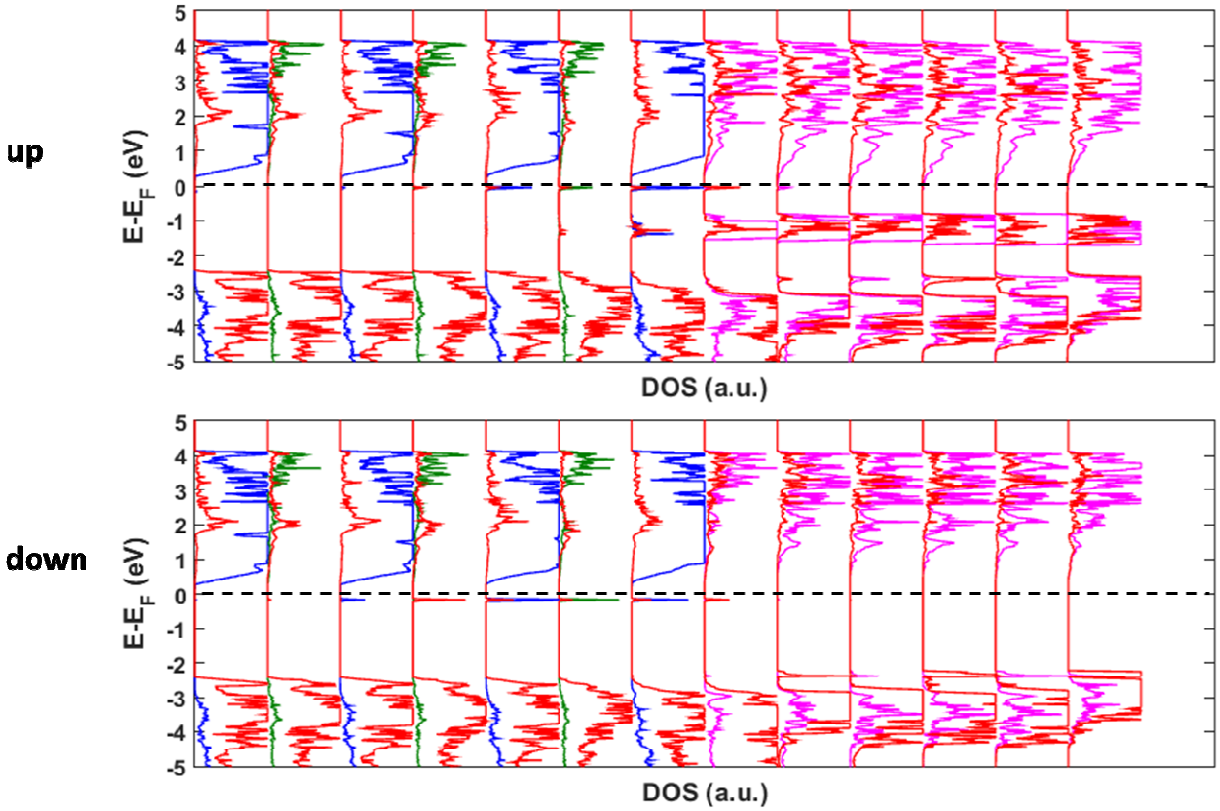

Figure 5